Journal of Catalysis **199,** 132–140 (2001)
doi:10.1006/jcat.2000.3153, available online at http://www.idealibrary.com on IDEAL®

Perovskites as Catalysts for the Selective Catalytic Reduction of Nitric Oxide with Propene: Relationship between Solid State Properties and Catalytic Activity

K. Kammer Hansen,*,†,[1] E. M. Skou,* H. Christensen,† and T. Turek‡

*Department of Chemistry, University of Southern Denmark, DK-5230 Odense M, Denmark; †Dinex Filter Technology A/S, DK-5500 Middelfart, Denmark; and ‡Department of Chemical Reaction Engineering, University of Karlsruhe, D-76128 Karlsruhe, Germany

Received October 2, 2000; accepted December 2, 2000; published online February 26, 2001

The influence of the solid state properties of manganese- and iron-based perovskites on the activity for the selective catalytic reduction of nitric oxide with propene under oxidizing conditions has been investigated. By substituting manganese for iron in the solid solution series $La_{0.6}Sr_{0.4}Fe_{1-y}Mn_yO_{3\pm\delta}$ ($0 \le y \le 1$) and by substituting strontium for lanthanum in the solid solution series $La_{1-x}Sr_xMnO_{3+\delta}$($0.05 \le x \le 0.50$) it is shown that the catalytic activity of the perovskites depends mainly on the redox properties of the transition metal and on the number of oxygen vacancies.

Key Words: **iron; manganese; nitric oxide; perovskite; propene.**

1. INTRODUCTION

The formation of NO_x (NO and NO_2) and N_2O from internal combustion engines is one of the undesirable side effects of modern society. In addition to being harmful to human beings, NO_x contributes to acid rain (1). N_2O is less harmful to human beings, but N_2O is a greenhouse gas (1). For the removal of NO_x under oxidizing conditions numerous systems have been developed (2). Among them the so-called selective catalytic reduction (SCR) process, using either hydrocarbon or ammonia as a reducing agent, is the most efficient (3). The most active catalysts for the SCR of nitric oxide with hydrocarbons are the transition metal–zeolites. Among the zeolites, Cu–ZSM (Zeolite Synthetic by Mobil) has the highest activity (4).

Several reaction mechanisms have been suggested to explain the SCR of nitric oxide with hydrocarbons (5–7). The mechanisms can be divided into two fundamentally different types. In the first type of mechanism the dissociation of nitric oxide on the catalyst surface is a crucial step. The role of the hydrocarbon is to restore the active sites on the catalyst surface by removing the adsorbed oxygen (5).

[1] To whom correspondence should be addressed. E-mail: kkh@chem.sdu.dk.

In the second type of mechanism the oxidation of nitric oxide with oxygen to reactive nitrogen dioxide is an essential intermediate reaction step. Nitrogen dioxide, which is more reactive than oxygen, reacts either directly with the hydrocarbon (6) or via an oxidized intermediate of the hydrocarbon formed on the catalyst surface (7). The second mechanism has gained the most attention. According to the second mechanism the catalyst must be able to catalyze both the *oxidation* of nitric oxide to nitrogen dioxide and the *reduction* of nitrogen dioxide to nitrogen with the hydrocarbon.

Perovskites can be very useful as model systems, especially because the perovskite matrix stabilizes a wide range of transition metals (8). Perovskites have the general formula $ABO_{3\pm\delta}$, where A is a large cation, i.e., La(III), Sr(II), or Ca(II), and B is a smaller cation, i.e., a transition metal. Perovskites of the form $A_{1-x}A'_xB_{1-y}B'_yO_{3\pm\delta}$ are particularly interesting. They provide an opportunity to control the oxidation state of the transition metal (the redox properties) and the oxygen stoichiometry (δ) by partial substitution of the A- and/or B-site cations. Among the perovskites the manganese-based perovskites are unique, as they are oxygen rich (9); that is, $\delta > 0$. To force the manganese-based perovskites to become oxygen deficient, another B-site cation can be substituted for manganese, i.e., iron (10).

Perovskites have been studied as catalysts for the direct decomposition of nitric oxide (11–15), the reduction of nitric oxide with carbon monoxide (16–18) or hydrogen (19, 20), and the SCR of nitric oxide with propene (21–24). Direct decomposition of nitric oxide on perovskites occurs only at high temperatures (above 600°C) and depends mainly on the number of oxygen vacancies and the B-site cation (25). The activity of the perovskites as catalysts for the decomposition of nitric oxide is significantly inhibited by oxygen. The activity of perovskites as catalysts for the reduction of nitric oxide with carbon monoxide or hydrogen increases with increasing temperature (18, 20). Only a few examples of perovskites useful as catalysts for

0021-9517/01 $35.00

the SCR of nitric oxide with carbon monoxide under oxidizing conditions are known (26). The reduction of nitric oxide with hydrogen on perovskites is nonselective with respect to oxygen. As catalysts for the SCR of nitric oxide with propene in the presence of oxygen, two different types of perovskites have been studied (21–24). The first type is the transition-metal-containing perovskites, $YFeO_3$ (21, 22) and $La_{0.59}Sr_{0.39}MnO_3$ (23). The second type is nontransition-metal-containing perovskites (24). The main advantage of perovskites as catalysts for the SCR of nitric oxide with propene is a high selectivity toward nitrogen with only minor amounts of nitrous oxide being formed (21–23). Perovskites in general have too low an activity for practical applications, but the activity can be significantly enhanced if they are supported on solid acids such as zirconia (21), sulfated zirconia (22), or alumina (23).

In this study the two solid solution series $La_{0.6}Sr_{0.4}Fe_{1-y}Mn_yO_{3\pm\delta}$, $y = 0.0, 0.2, 0.4, 0.6, 0.8$, and 1.0 (LSFM000–LSFM100, series 1) and $La_{1-x}Sr_xMnO_{3+\delta}$, $x = 0.05$, 0.15, 0.25, 0.35, and 0.50 (LSM5–LSM50, series 2) were synthesized and characterized by X-ray powder diffraction, temperature-programmed reduction (TPR), and BET surface area measurements. The activity of the perovskites as catalysts for the SCR of nitric oxide with propene under oxidizing conditions is compared in order to correlate the solid-state properties of the perovskites with the catalytic activity.

2. EXPERIMENTAL

2.1. Synthesis. The first solid solution series, LSFM000–LSFM100, was synthesized by an aqueous citric acid route using nitrates as starting materials (27). Aqueous solutions of the metal–nitrates were made in the following way. Two hundred grams of $Mn(NO_3)_2 \cdot 4H_2O$ (Merck, >97%) was dissolved in 56 g of boiled distilled water, 126 g of $Fe(NO_3)_3 \cdot 9H_2O$ (Merck, +99%) was dissolved in 250 g of boiled distilled water, 135 g of $La(NO_3)_3 \cdot 6H_2O$ (Chempur, +99%) was dissolved in 108 g of boiled distilled water, and 85 g of $Sr(NO_3)_2$ (BDH, >99.5%) was dissolved in 180 g of boiled distilled water. All the solutions were made less than saturated (20% excess of water) to avoid precipitation of the metal ions during storage. The exact amounts of metal ions in the solutions were determined by thermogravimetry as follows. Approximately 0.04 g of the samples was placed in an open-ended alumina crucible. The samples were then transferred to a Setaram TG92-12 thermobalance. The Mn solution was heated at 1000°C in 1% hydrogen in argon for 5 h and the amount of manganese in the solution was determined as MnO. The Fe and La solutions were both heated at 1000°C in 50% oxygen in nitrogen for 5 h, and the amounts of iron and lanthanum in the solutions were determined as Fe_2O_3 and La_2O_3. The Sr solution was heated at 140°C for 5 h in 50% oxygen in nitrogen, and the amount of strontium was determined by assuming that all strontium was in the form of $Sr(NO_3)_2$. The synthesis of the LSFM perovskites was carried out using the above solutions. The molar amounts of the solutions were mixed in a beaker and diluted to 100 ml with distilled water. Double the molar amount of citric acid (Merck, +99.5%) was added to the solution. After the solution was heated to 80°C, polyethylene glycol (Merck) was added. The solvent was evaporated slowly before the powder was transferred to an alumina crucible. The powder was heated at 400°C for 3 h in air. All the powders were finally calcined at 600°C in air.

The second solid solution series, LSM5–LSM50, was synthesized by spray pyrolysis using glycine complexes. Aqueous solutions of the metal–nitrates were made as above. The amounts of metal ions in the solutions were determined by traditional gravimetry. The metal–nitrate solutions were mixed in the molar amounts and glycine was added as a chelating agent. The synthesis was performed in a drip pyrolysis furnace described elsewhere (28). All powder samples were calcined at 600°C in air for 1 h before use.

2.2. Characterization. The powders were characterized by X-ray powder diffraction using a Siemens D5000 diffractometer with Cu$K_{\alpha 1}$ radiation. The powder patterns were recorded between a 2θ of 10° and 80° with a step size of 0.02°.The PC-DOS program TREOR90 was used to determine the crystal system (29). The BET surface areas of the perovskite powders were determined with a Micromeritics Flowsorb II 2300. The powders were degassed at 110°C for 1 h before the measurements. TPR was performed on a Micromeritics Autochem 2910 using 0.2 g powder. Before the TPR measurements the powders were pretreated in a flow of oxygen at 600°C for 2 h. The powders were then cooled to 100°C before being heated to 1050°C, with a heating rate of 10°C min^{-1} in 4% hydrogen in nitrogen. The gas-phase products formed during the reduction were detected with a thermal conductivity detector (TCD). The products after the TPR measurements were characterized by X-ray powder diffraction.

2.3. Catalytic measurements. A fixed-bed reactor was used for measurements of catalytic activity. Before the measurements the powders were shaped as microcylinders by cold pressing and crushing. The cylinders were sieved to obtain a catalyst with a grain size of 0.315 to 0.500 mm. For characterization of the catalytic activity 1.5 g of powder was used.

For gas-phase analysis the following equipment was used. Oxygen was detected with a Hartmann & Braun Magnos 6G paramagnetic analyzer; CO, CO_2, NO, and N_2O were all detected with Leybold–Heraeus Binos nondispersive IR analyzers. For detection of NO_2 a Tecan CLD 502 NO/NO_x chemiluminescence analyzer was used. The analyzers were calibrated using calibration gases from Messer and the

analyzers were controlled and adjusted for possible cross-selectivity before use. The inlet concentration of propene was determined by assuming a 100% conversion of propene to carbon dioxide at 600°C. The amount of nitrogen formed during the reduction of nitric oxide was calculated from a nitrogen mass balance.

The composition of the inlet gas was 4% oxygen, 1000 ppm nitric oxide, and 1000 ppm propene with balance helium. All gases were from Messer and were used as received without further purification. A space velocity of approximately 8000 h^{-1} was used throughout the measurements. The composition of the inlet gas was controlled by four Brooks 5850E series mass flow controllers. The measurements were conducted from 500°C to 200/250°C with the temperature decreased in steps of 50°C. Additional measurements were performed on some of the compounds at 325 and 375°C. Steady state was normally achieved within 2 h. Before the measurements the catalyst was pretreated in helium at 600°C for 1 h to ensure that all the catalysts had the same surface oxidation state. Additional measurements with varying inlet concentrations of propene and oxygen were performed on LSFM100 to gain additional information on the mechanism of the nitric oxide reduction by propene.

3. RESULTS

3.1. X-xay. The results from the X-ray powder diffraction measurements are summarized in Table 1 and denoted by their crystal systems. All the iron-containing perovskites could be indexed using an orthorhombic unit cell. LSM50 is also orthorhombic, whereas the rest of the LSM series and LSFM100 could be indexed in a hexagonal unit cell. No additional lines were found in the powder patterns.

3.2. BET. For the LSFM series the BET surface area varies from 13 to 20 $m^2\ g^{-1}$; see Table 1. The perovskites

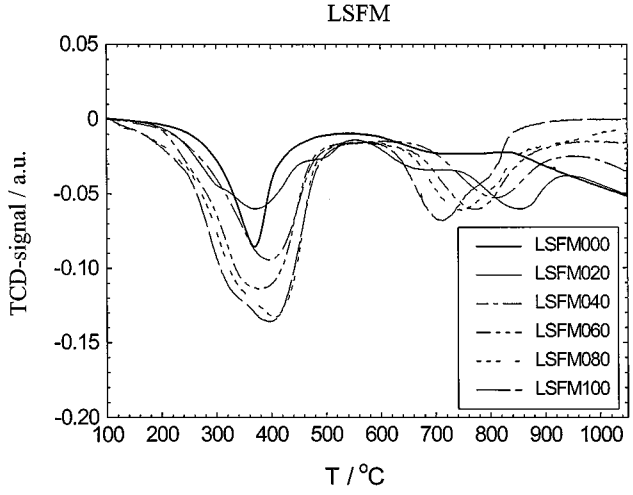

FIG. 1. Temperature-programmed reduction on series 1 in 4% hydrogen in nitrogen.

LSFM40 and LSFM60 have the largest surface areas, the end products of the solid solution series LSFM000 and LSFM100 the smallest. The BET surface areas of the LSM powders are slightly smaller than the surface areas of the LSFM powders and the surface area decreases from 15 to 7 $m^2\ g^{-1}$ with increasing strontium content.

3.3. TPR. In Fig. 1 the results from the TPR measurements on series 1 are shown. In general the reduction of the perovskites proceeds in two steps. The first reduction peak has its minimum around 400°C. For LSFM100 the first reduction peak is split into two. The second reduction peak is placed at a much higher temperature and depends on the composition of the perovskite. When the amount of manganese increases, the temperature for the second reduction is decreased from 800 to 700°C. The perovskite matrix is destroyed after the second reduction. X-ray powder

TABLE 1

Solid-State and Catalytic Properties of LSFM- and LSM-Based Perovskites

Composition	Crystal system	BET ($m^2\ g^{-1}$)	Max. conversion of NO to N_2 (%) (10^{-6} mol $m^{-2}\ s^{-1}$)	Temperature of Max NO to N_2 conversion (°C)	Temperature of 100% propene oxidation (°C)
LSFM000	Orthorhombic	13.4	16.0 (6.51)	350	400
LSFM020	Orthorhombic	14.9	17.8 (6.52)	350	350
LSFM040	Orthorhombic	17.1	22.2 (7.08)	350	350
LSFM060	Orthorhombic	19.7	26.3 (7.29)	350	350
LSFM080	Orthorhombic	18.7	33.2 (9.69)	325	325
LSFM100	Hexagonal	16.6	34.4 (11.3)	325	300
LSM05	Hexagonal	14.6	19.9 (7.42)	350	325
LSM15	Hexagonal	11.0	19.4 (9.62)	400	400
LSM25	Hexagonal	10.0	20.3 (11.1)	325	325
LSM35	Hexagonal	8.9	22.6 (13.9)	325	325
LSM50	Orthorhombic	7.0	31.1 (24.2)	325	300

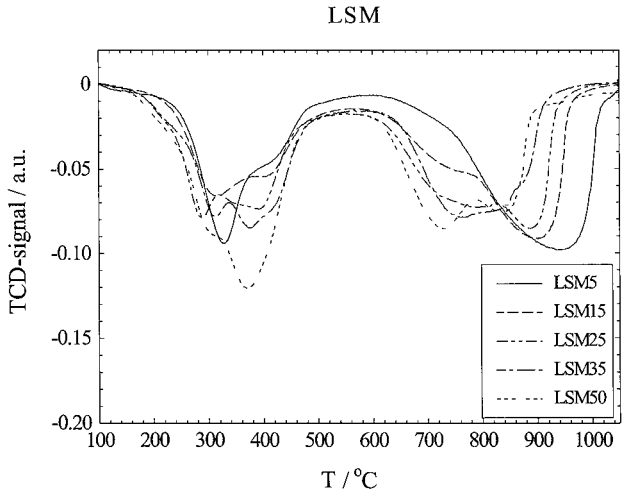

FIG. 2. Temperature-programmed reduction on series 2 in 4% hydrogen in nitrogen.

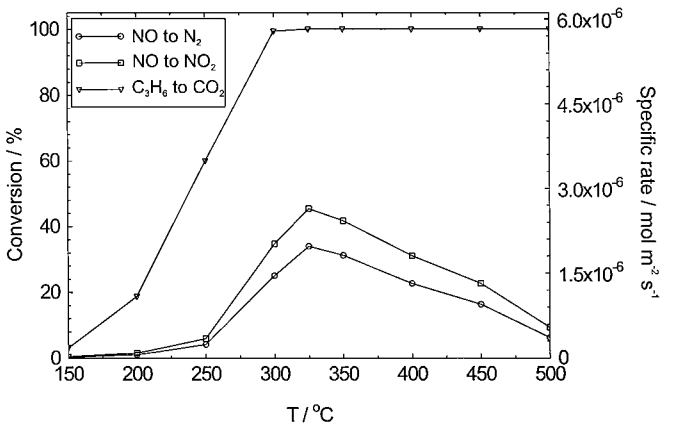

FIG. 3. The oxidation of propene to carbon dioxide and the conversion of nitric oxide to nitrogen and to nitrogen dioxide on LSM35 as a function of temperature.

diffraction reveals that mixtures of SrO, MnO, La_2MnO_4, and Fe_2O_3 are obtained after the TPR measurements. Figure 2 contains in a similar fashion the results from the TPR measurements on the second solid solution series. The TPR spectra are more complex than those for series 1. For the hexagonal phases the first reduction peak is split into two just as it is for LSFM100. The second reduction peak is likewise split into two for all compounds except LSM5. The temperature for the final reduction decreases with increasing strontium content. X-ray powder diffraction gives SrO, MnO, and La_2MnO_4 as the products after the TPR measurements.

3.4. Catalytic measurements. As an example of the reduction of nitric oxide with propene the results from the measurements on LSM35 are shown in Fig. 3. The behavior of LSM35 is as observed in the SCR process when propene is used as a reducing agent (30). A sharp increase in the reduction of nitric oxide is observed shortly before the temperature of maximum conversion of nitric oxide to nitrogen is reached. The maximum conversion of nitric oxide is only observed in a narrow temperature range and the conversion of nitric oxide to nitrogen decreases abruptly at higher temperatures when entering the so-called "equilibrium" region. No formation of nitrous oxide is observed (<10 ppm) on any of the catalysts tested in the temperature range covered. The oxidation of propene to carbon dioxide on LSM35 as a function of temperature is likewise shown in Fig. 3. The oxidation of propene is initiated at around 150–200°C and increases until a steady-state conversion of propene to carbon dioxide is reached at 300–400°C depending on the nature of the perovskite. No formation of carbon monoxide is detected (<10 ppm) on any of the catalysts tested in the temperature range covered. The amount of nitric oxide converted to nitrogen dioxide (the measured concentration of NO_2 in the outlet gas steam) is also shown in Fig. 3. In Table 1 the maximum conversion of nitric oxide to nitrogen, the temperature at which the conversion of nitric oxide to nitrogen is at maximum, and the temperature at which a 100% conversion of propene to carbon dioxide is achieved are presented for all the catalysts. It is observed that the maximum conversion of nitric oxide to nitrogen in general is reached at the same temperature, at the temperature of 100% propene conversion. All catalysts deactivated when the catalysts were kept at temperatures below the temperature of 100% conversion of propene for a prolonged time. Heating the catalyst at 600°C in 4% oxygen in helium restored the activity of the catalysts.

In Fig. 4 the maximum conversion of nitric oxide to nitrogen for series 1 and 2 is shown as a function of the

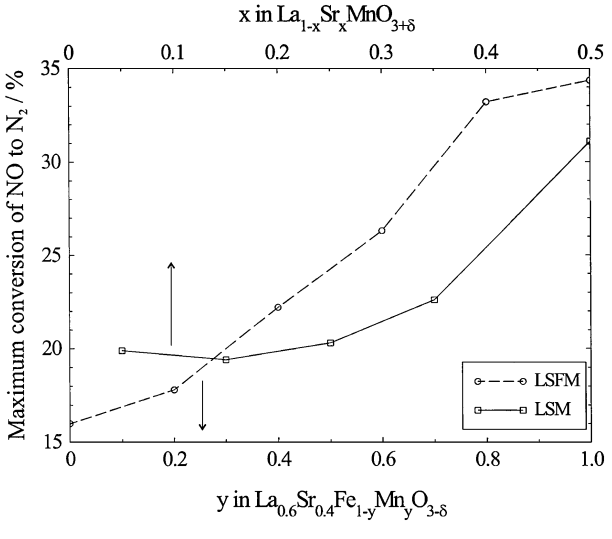

FIG. 4. Maximum conversion of nitric oxide to nitrogen as a function of x in $La_{1-x}Sr_xMnO_{3+\delta}$ and as a function of y in $La_{0.6}Sr_{0.4}Fe_{1-y}Mn_yO_{3\pm\delta}$.

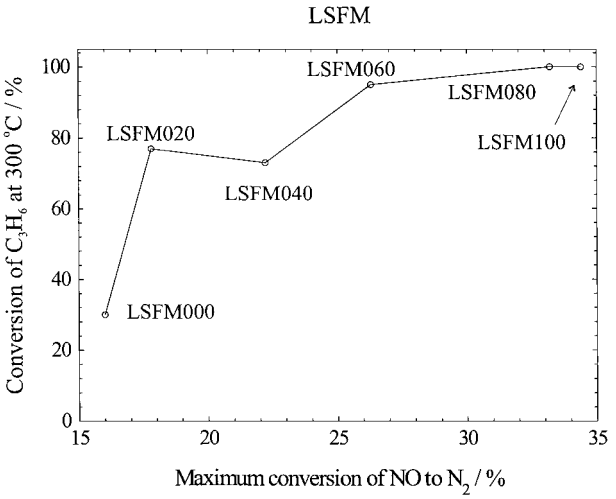

FIG. 5. The conversion of propene to carbon dioxide at 300°C as a function of the maximum conversion of nitric oxide to nitrogen on series 1.

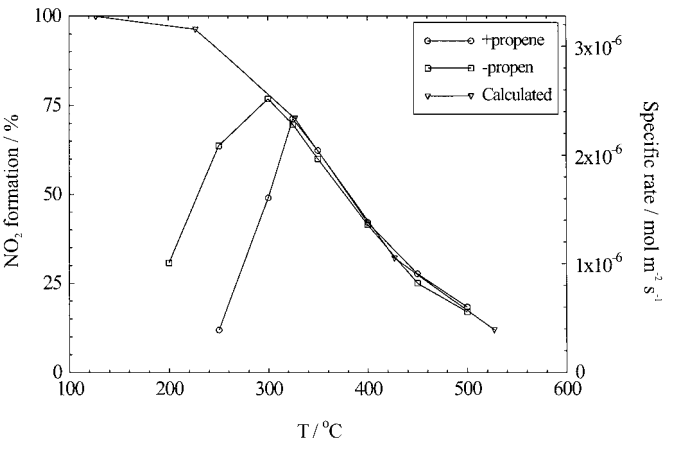

FIG. 6. The calculated and measured amount of nitrogen dioxide formed on LSFM100 as a function of temperature in a 4% oxygen and 1000-ppm nitric oxide in helium gas mixture with 1000 ppm propene (+propene) and without propene (−propene).

manganese and strontium contents, respectively. It can be seen that the conversion of nitric oxide to nitrogen increases from 16% for LSFM000 to 34% for LSFM100. The conversion of nitric oxide to nitrogen as a function of the strontium content in LSM shows that as long as the strontium content is kept below 0.35 no difference is observed in the catalytic activity of the LSM compounds. However, when the strontium content is increased above 0.35 the conversion of nitric oxide to nitrogen increases from about 20 to 31%.

A comparison of the oxidation of propene to carbon dioxide at 300°C as a function of the maximum conversion of nitric oxide to nitrogen for the solid solution series LSFM can be seen in Fig. 5. There is clearly a positive relationship between the oxidation of propene to carbon dioxide and the maximum conversion of nitric oxide to nitrogen.

A series of measurements without propene (1000 ppm nitric oxide and 4% oxygen in helium) was conducted on LSFM100 as a function of temperature. The measured amount of nitrogen dioxide formed was compared with the calculated amount of nitrogen dioxide formed in the presence of 1000 ppm propene, under the assumption that all nitric oxide removed as nitrogen is oxidized to nitrogen dioxide before reacting with propene (see Fig. 6). For comparison the calculated equilibrium concentration of nitrogen dioxide in a 1000-ppm nitric oxide and 4% oxygen in helium gas mixture is plotted. For the calculations data from Ref. (31) were used. A good agreement between the three curves is observed above approximately 250°C.

In Fig. 7 the results obtained by varying the inlet concentration of propene on LSFM100 at 325 and 350°C are shown. The amount of nitrogen dioxide formed, calculated from the assumption that all nitric oxide reduced to nitrogen is oxidized to nitrogen dioxide before reacting with propene, is also shown in Fig. 7. At 325°C the conversion of nitric oxide to nitrogen increases slightly when the concentration of propene is increased from 500 to 1000 ppm. A further increase in the inlet concentration of propene does not lead to an increase in the conversion of nitric oxide to nitrogen. In fact, the conversion of nitric oxide to nitrogen even decreases. It is seen that the formation of nitrogen dioxide is suppressed when the inlet concentration of propene is increased. At inlet concentrations of propene higher than 2000 ppm the combustion of propene was incomplete and deactivation of the catalyst occurred before steady state was achieved. At higher temperatures, shown for LSFM100 at 350°C in Fig. 7, the conversion of nitric oxide to nitrogen increased weakly with increasing concentration of propene. At inlet concentrations of propene higher than 2500 ppm the oxidation of propene was incomplete and deactivation of the catalyst was observed.

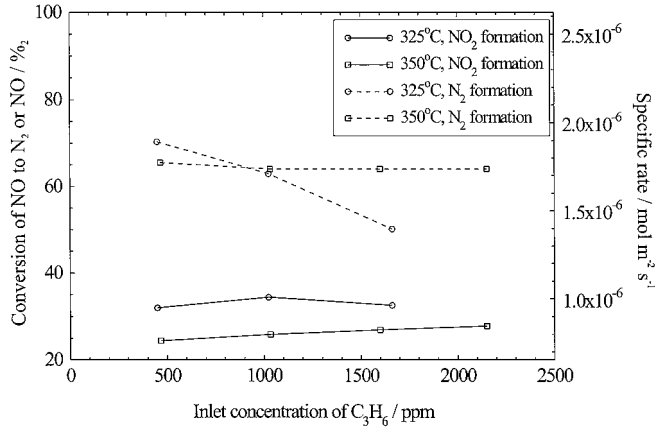

FIG. 7. The conversion of nitric oxide to nitrogen (solid line) and the total amount of nitrogen dioxide formed (dashed line) as a function of the inlet concentration of propene on LSFM100 at 325 and 350°C.

When the inlet concentration of oxygen was below 1% at 325°C rapid deactivation of the catalyst was observed, and the activity increased significantly when oxygen was added to the inlet gas. For an inlet concentration of oxygen greater than 1%, no significant change in the catalytic activity was observed.

4. DISCUSSION

4.1. X-ray. The powder patterns for the two solid solution series reveal that all the synthesized perovskite powders are single phases. For series 2 the variation from a hexagonal to an orthorhombic unit cell with increasing strontium content is as expected (32).

4.2. TPR. The first reduction peak observed in the TPR spectra for the series 1 powders is due to the reduction of Mn(IV) to Mn(III) and/or Fe(IV) to Fe(III) (33). However, for LSFM100 the first reduction peak is clearly split into two. This is most likely due to a two-step reduction where the first reduction peak corresponds to the reduction of Mn(IV) in the hexagonal phase under the formation of an orthorhombic phase; see the discussion of the TPR measurements done on series 2. The other compounds show only a very weak splitting of the first peak. The second reduction peak is due to the reduction of Mn(III) to Mn(II) as X-ray powder diffraction shows MnO and La_2MnO_4 as the reduction products. For LSFM000 the reduction is incomplete even at 1050°C.[2] This is confirmed by X-ray powder diffraction, as the powder pattern contains reflections due to hematite (α-Fe_2O_3) and not to wüstite (FeO). As it is difficult to reduce Fe(IV)/Fe(III) to Fe(II)/Fe(0) in oxides this is as expected. By plotting the difference in temperature, $\triangle T$, between the two reduction peaks (estimated for LSFM000) as a function of the manganese content, a clear correlation between $\triangle T$ and the manganese content is observed (see Fig. 8). When manganese is substituted for iron, the difference in temperature between the two reduction peaks decreases from 500 to 320°C. The smaller the temperature difference, the closer in energy Mn(IV)/Mn(III) is to Mn(III)/Mn(II) and the lower the relative position of the Fermi level will be (the system is more oxidized). The manganese-rich perovskites are, in other words, stronger oxidizing agents than the iron-rich perovskites. When manganese is substituted for iron, the oxygen stoichiometry of the perovskites will increase as the defect equilibrium (using the Kröger–Vink notation)

$$\mathrm{Fe}^{*}_{\mathrm{Fe}} \rightarrow \mathrm{Fe}^{*}_{\mathrm{Fe}} + e' \qquad [1]$$

is displaced further to the left than the defect equilibrium

$$\mathrm{Mn}^{*}_{\mathrm{Mn}} \rightarrow \mathrm{Mn}^{\bullet}_{\mathrm{Mn}} + e'. \qquad [2]$$

[2] The maximum operating temperature for the TPR instrument is 1050°C.

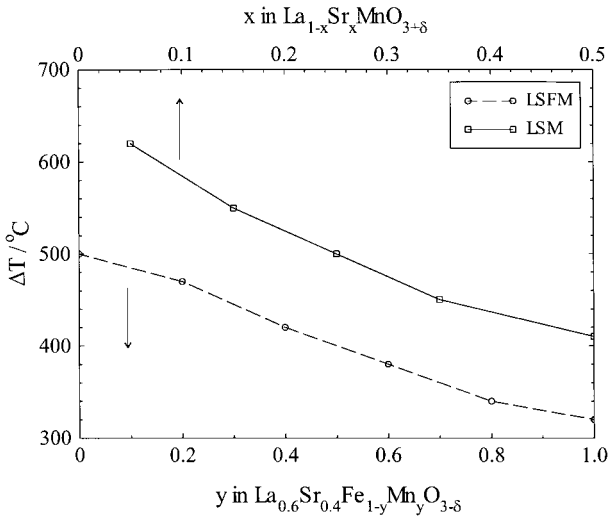

FIG. 8. The temperature difference between the first and the last reduction peak, as determined by the TPR measurements, as a function of x in $La_{1-x}Sr_xMnO_{3+\delta}$ and as a function of y in $La_{0.6}Sr_{0.4}Fe_{1-y}Mn_yO_{3+\delta}$.

Because the only possibility of charge compensation for the oxidation of the transition metal is an adjustment of the oxygen stoichiometry, the stoichiometry will decrease with increasing iron content (the oxygen vacancy concentration will increase). By classical wet chemical analysis (32) it has been shown that only LSFM000 and LSFM020 are oxygen deficient in air. When the manganese content is 0.4 or higher, the perovskites become stoichiometric (34). The ratio between lanthanum and strontium in the LSFM series is therefore chosen such that all the perovskites are either stoichiometric or oxygen deficient. All the LSFM perovskites will therefore contain a considerable number of oxygen vacancies.

For the second solid solution series the first reduction peak is split into two for the hexagonal phases. This is probably due to a two-step reduction, where the first reduction is the reduction of Mn(IV) in the hexagonal phase to Mn(III) under the formation of an orthorhombic (stoichiometric) phase. The remaining Mn(IV) in the orthorhombic phase is then reduced to Mn(III). The second reduction peak is due to the reduction of Mn(III) to Mn(II) as confirmed by X-ray powder diffraction. Whether the splitting of the second reduction peak for LSM15, LSM25, LSM35, and LSM50 is due to incomplete reduction of Mn(III) is not clear. Upon substituting strontium for lanthanum behavior similar to that observed for the LSFM series is found. This is illustrated in Fig. 8, where the temperature difference between the first and the last reduction peak is plotted as a function of the strontium content. The temperature difference between the two reduction peaks clearly decreases as a function of increasing strontium content. This is in agreement with literature data from thermogravimetric analysis showing that high-strontium-substituted LSM is reduced easier

than low-strontium-substituted LSM (35). The Fermi level of the LSM perovskites decreases therefore as a function of increasing strontium doping. It is known that the oxygen stoichiometry of the LSM perovskites decreases with increasing strontium content under the formation of oxygen vacancies (see below (36)). The point is, however, that the redox properties of the LSM perovskites are substantially changed as well. This can be illustrated as follows. By substituting strontium for lanthanum two ways of charge compensation exist (using the Kröger–Vink notation):

$$O_O^* \rightarrow V_O^{\bullet\bullet} + 2e' + 1/2O_2(g) \quad [3]$$

or

$$Mn_{Mn}^* \rightarrow Mn_{Mn}^{\bullet} + e'. \quad [2]$$

As shown by Krogh Andersen *et al.* (32), both a decrease in the oxygen stoichiometry and the oxidation of Mn(III) to Mn(IV) occurs. That is, the higher the strontium content, the lower the oxygen stoichiometry and the higher the Mn(IV) content. It has been shown that the oxygen stoichiometry decreases until the perovskite becomes stoichiometric ($\delta = 0$) at $x = 0.3$. Above $x = 0.3$ the oxygen stoichiometry is nearly constant and only the oxidation of Mn(III) to Mn(IV) occurs (32). When the LSM perovskites are oxygen rich ($\delta > 0$) there will only be very few oxygen vacancies in the structure. When x exceeds 0.3 the perovskite becomes stoichiometric and the number of oxygen vacancies in the structure increases upon further strontium substitution. Series 2 is therefore chosen so that the perovskites change from having only a limited number of oxygen vacancies ($x < 0.3$) to having a considerable amount of oxygen vacancies ($x > 0.3$). A substitution of strontium for lanthanum will therefore decrease the Fermi level of the LSM-based perovskites, making them stronger oxidizing agents and creating oxygen vacancies in the structure.

4.3. Catalytic activity. As seen in Fig. 6 the calculated and measured curves for the formation of nitrogen dioxide coincide very well above the temperature of maximum conversion of nitric oxide to nitrogen. At the same time, nitrogen dioxide is observed in the outlet gas (see Fig. 3). This is in agreement with a mechanism where nitric oxide is oxidized to nitrogen dioxide before reacting with propene. The low activity and the rapid deactivation of the catalyst observed in the measurement without the oxygen needed for the oxidation of nitric oxide to nitrogen dioxide further support this. A mechanism where the dissociation of nitric oxide on the catalyst surface is an intermediate reaction step is less likely on perovskites. Decomposition of nitric oxide on perovskites has only been observed at temperatures above 600°C (11). Therefore, it is not expected that any activity at temperatures as low as 325°C on the background of this type of mechanism will be observed. On the contrary it should be expected that the conversion of nitric oxide to nitrogen would increase above temperatures of 500°C and not, as is the case, decrease. Furthermore dissociation of nitric oxide is inhibited by oxygen (14). This is in contrast to the need for oxygen in the feed gas, as oxygen enhances the reduction rate. Above the temperature of the maximum conversion of nitric oxide to nitrogen, the conversion therefore decreases as the formation of nitrogen dioxide is limited by the strongly temperature-dependent equilibrium:

$$NO + 1/2O_2 \leftrightarrow NO_2. \quad [4]$$

In Fig. 6 it is seen that, at temperatures below approximately 250°C, the amount of nitrogen dioxide formed is significantly lower than the calculated equilibrium value. The kinetics for the oxidation of nitric oxide to nitrogen dioxide are insufficient for reaching the equilibrium concentration of nitrogen dioxide at low temperatures. When the amounts of nitrogen dioxide formed in the experiments with and without propene are compared, it is observed that below the temperature of maximum reduction of nitric oxide to nitrogen the formation of nitrogen dioxide is inhibited in the presence of propene. At the same time it is observed that an increase in the inlet concentration of propene does not increase the conversion of nitric oxide to nitrogen (see Fig. 7). If the amount of nitrogen dioxide is calculated, under the assumption that all nitric oxide removed as nitrogen is oxidized to nitrogen dioxide before reacting with propene at 325°C, it is observed that the formation of nitrogen dioxide decreases with increasing inlet concentration of propene (see Fig. 7). This indicates that the active sites are poisoned by propene or partially oxidized propene-derived species, suppressing the oxidation of nitric oxide to nitrogen dioxide. On this background it is likely that, at temperatures above the temperature of maximum conversion of nitric oxide to nitrogen, the reduction of nitric oxide is limited primarily by the equilibrium-controlled amount of nitrogen dioxide formed. At temperatures below the maximum conversion of nitric oxide to nitrogen, the low activity of the perovskites for the oxidation of propene results in inhibition of the active sites by propene. This limits the formation of nitrogen dioxide, leading to a decrease in the activity for nitric oxide reduction. The maximum conversion of nitric oxide to nitrogen is then mainly determined by the temperature of the propene light off. If the temperature for the propene light off is low, the measured concentration of nitrogen dioxide will intersect the nitrogen dioxide equilibrium curve at a low temperature, where the thermodynamicly determined concentration of nitrogen dioxide is high (see Fig. 6). If the temperature of the propene light off is high, on the other hand, the measured concentration of nitrogen dioxide will intersect the nitrogen dioxide equilibrium curve at a higher temperature, where the thermodynamicly determined concentration of nitrogen dioxide is low. The correlation between the kinetics of the oxidation of propene and the reduction of nitric oxide (see Fig. 5)

further underlines this. When the catalyst has a high activity for the oxidation of propene the activity for nitric oxide decomposition is high. Therefore, at low temperatures, the data suggest that the rate-limiting step is the oxidation of propene.

It is important to note that no nitrous oxide is formed during the decomposition of nitric oxide. This is in agreement with the literature (21–23). The high selectivity toward nitrogen is apparently a common property of perovskites.

A higher activity (three to four times higher) is observed in this study than is reported in the literature (21–23). However, the reaction conditions reported in the literature were slightly less optimal, as a higher space velocity was used (two to three times higher). Also it should be noted that the catalytic activity depends on the synthesis conditions. In this work the activity of the perovskites synthesized by the citric acid method was slightly greater than that of the perovskites synthesized by spray pyrolysis. As stated in the Introduction the activity of the perovskites is much too low for practical applications. Compared on the background of space velocity alone the activity is a factor of 5 to 10 too low (37). However, this work has shown that the catalytic activity can be enhanced by proper choice of the composition of the perovskites. Also work reported in the literature has shown that an increase in the activity can be achieved by supporting the perovskites on solid acids (21–23). The deactivation of the catalysts observed at temperatures below complete combustion of propene is a common problem encountered when an unsaturated hydrocarbon is used as a reducing agent (38).

4.4. Correlation between solid state properties and catalytic activity. By substituting manganese for iron, a higher activity for the reduction of nitric oxide is achieved. As explained by the TPR measurements, the manganese-rich perovskites have a lower lying Fermi level than the iron-rich perovskites. In other words, the manganese-rich perovskites are stronger oxidizing agents. As the exact reaction mechanism for the SCR process is unknown, it is difficult to correlate the redox properties directly to the catalytic properties of the perovskites. However, the need for the perovskites to be strong oxidizing agents indicates that a rate-limiting step in the SCR process is an oxidation step, i.e., the oxidation of nitric oxide to nitrogen dioxide or the oxidation of propene.

For the second solid solution series, LSM, no or only a slight effect is observed by substituting strontium for lanthanum below a strontium content of 0.35. The catalytic activity for the removal of nitric oxide then increases. As the Fermi level decreases with increasing strontium doping, the catalytic activity should increase if only the redox properties are determining the activity, just as is observed for the LSFM series. As LSM5, LSM15, and LSM25 all are oxygen rich, they contain only a very limited number of oxygen vacancies. This indicates that the presence of oxygen vacancies is an important parameter for determining the activity of the perovskites as a catalyst in the SCR process. When the perovskites contain a very limited number of oxygen vacancies, the catalytic activity is limited by the number of oxygen vacancies. When the perovskites becomes stoichiometric, that is, when $x > 0.3$, the number of oxygen vacancies increases and the catalytic activity increases as well. This indicates that the number of oxygen vacancies in the perovskite structure in part determines the number of active sites. As x in the LSFM series is 0.4, the number of oxygen vacancies in the LSFM perovskites is high, and the number of oxygen vacancies therefore does not limit the rate. So the catalytic activity is determined both by the number of oxygen vacancies and by the redox properties of the perovskites.

It is noteworthy that the redox capacity (the percentage of the total amount of manganese participating in a possible redox cycle) has only a minor effect on the catalytic activity of the perovskites. The redox capacity decreases strongly with increasing strontium doping, becoming almost zero for LSM25 (32). Work reported on metallosilicates has, on the other hand, shown that a high redox capacity is necessary for achieving a high catalytic activity (39). As the redox capacity of perovskites only has a minor influence on the catalytic activity, this indicates that the rate-limiting step is different on zeolites and perovskites. Many authors have suggested that the SCR of nitric oxide on zeolites proceeds with the decomposition of nitric oxide on the catalyst surface as an intermediate reaction step (39–41). This indicates that if the redox capacity is responsible for the catalytic activity, the decomposition of nitric oxide is an intermediate reaction step. If, on the other hand, the oxidizing strength is crucial for the catalytic activity, as on perovskites, the oxidation of nitric oxide to nitrogen dioxide is an intermediate reaction step. The catalytic activity is therefore determined by different properties.

In conclusion, the parameters of greatest importance for the catalytic activity are the relative position of the Fermi level and the number of oxygen vacancies. A possible redox cycle is not rate-limiting.

5. CONCLUSION

Perovskites have been investigated as catalysts for the selective catalytic reduction of nitric oxide with propene. The perovskites have a high selectivity toward nitrogen and carbon dioxide, but the activity for the reduction of nitric oxide is too low for nonstationary applications. The SCR process on perovskites follows most likely a reaction pathway where the oxidation of nitric oxide to nitrogen dioxide is an intermediate reaction step. The data indicate that the oxidation of propene is rate-limiting at low temperatures.

The activity of the perovskites is primarily determined by the redox properties of the perovskites. TPR data confirm

that the stronger the oxidizing ability of the perovskite, the higher the activity of the perovskite. This suggests that the rate-limiting step on perovskites is an oxidation process, i.e., the oxidation of nitric oxide to nitrogen dioxide or the oxidation of propene. The number of oxygen vacancies primarily determines the number of active sites. The redox capacity has only a minor influence on the catalytic activity of the perovskites.

ACKNOWLEDGMENTS

The authors thank Lene Kragelund for synthesis of the $La_{0.6}Sr_{0.4}Fe_{1-y}Mn_yO_{3\pm\delta}$ series and Steen S. Nissen and Ninette Kjerulf-Jensen for synthesis of the $La_{1-x}Sr_xMnO_{3+\delta}$ series. One of the authors (K. Kammer Hansen) greatly acknowledges the Danish Academy of Technical Science for financial support.

REFERENCES

1. Manahan, S. E., "Environmental Chemistry," 6th, ed., P. 338. CRC Press, London, 1994.
2. Fritz, A., and Pitchon, V., *Appl. Catal. B: Environ.* **13**, 1 (1997).
3. Pârvulescu, V. I., Grange, P., and Delmon, B., *Catal. Today* **46**, 233 (1998).
4. Iwamoto, M., and Yahiro, H., *Catal. Today* **22**, 5 (1994).
5. Yogo, K., Tanaka, S., Ihara, M., Hishiki, T., and Kikuchi, E., *Chem. Lett.* 1025 (1992).
6. Ukisu, Y., Sato, S., Abe, A., and Yoshida, K., *Appl. Catal. B: Environ.* **2**, 147 (1993).
7. Burch, R., and Scire, S., *Catal. Lett.* **27**, 177 (1994).
8. Yamazoe, H., and Teraoka, Y., *Catal. Today* **8**(2), 175 (1990).
9. Misusaki, J., Mori, N., Takai, H., Yonemura, Y., Minamiue, H., Tagawa, T., Dokiya, M., Inaba, H., Naraya, K., Sasamoto, T., and Hashimoto, T., *Solid State Ionics* **129**, 163 (2000).
10. Kindermann, L., Das, D., Nickel, H., and Hilpert, K., *Solid State Ionics* **89**, 215 (1996).
11. Shin, S., Arakawa, H., Hatakeyama, Y., Ogawa. K., and Shimomura, K., *Mater. Res. Bull.* **14**, 633 (1979).
12. Shimada, H., Miyama, S., and Kuroda, H., *Chem. Lett.* 1797 (1988).
13. Teraoka, Y., Fukuda, H., and Kagawa, S., *Chem. Lett.* 1 (1990).
14. Teraoka, Y., Harada, T., and Kagawa, S., *J. Chem. Soc. Faraday Trans.* **94**(13), 1887 (1998).
15. Yokoi, Y., and Uchida, H., *Catal. Today* **42**, 167 (1998).
16. Öcal, M., Oukaci, R., Marcelin, G., and Agarwal, S. K., *Ing. Eng. Chem. Res.* **33**, 2930 (1994).
17. Forni, L., Oliva, C., Barzetti, T., Selli, E., Ezerets, A. M., and Vishiniakov, A. V., *Appl. Catal. B: Environ.* **13**, 35 (1997).
18. Teraoka, Y., Nii, H., Kagawa, S., Jansson, K., and Nygren, M., *J. Mater. Chem.* **6**(1), 97 (1996).
19. Linstedt, A., Strömberg, D., and Milh, M. A., *Appl. Catal. A: Gen.* **116,** 109 (1994).
20. Ferri, D., Forni, L., Dekkers, M. A. P., and Nieuwenhuys, B. E., *Appl. Catal. B: Environ.* **16**, 339 (1998).
21. Lentmaier, J., Kemmler-Sack, S., Knell, G., Kessler, P., and Plies, E., *Mater. Res. Bull.* **31**, 1269 (1996).
22. Lentmaier, J., and Kemmler-Sack, S., *Mater. Res. Bull.* **33**, 46 (1998).
23. Menezo, J. C., Inkari, S., Bertin, T., Barbier, J., Davias-Bainier, N., Noirot, R., and Seguelong, T., *Appl. Catal. B: Environ.* **15**, L1 (1998).
24. Furukawa, H., Harada, T., Teraoka, Y., and Kagawa, S., "68th Meeting of the Catalysis Society of Japan (A)," p. 4H215, 1991.
25. Zhao, Z., Yang, X., and Wu, Y., *Appl. Catal. B.: Environ.* **8**(4), 281 (1996).
26. Bradow, R., Jovanovic, D., Petrovic, S., Jovanovic, Z., and Terlecki-Baricevic, A., *Ing. Eng. Chem. Res.* **34**, 1929 (1995).
27. Wu, Y., Zhao, Z., and Yang, X., *Appl. Catal. B: Environ.* **8**(3), 281 (1996).
28. Gordes, P., Christiansen, N., Jensen, E. J., and Villadsen, J., *J. Mater. Sci.* **30**(4), 1053 (1995).
29. Werner, P.-E.,"Treor," Department of Structural Chemistry, University of Stockholm, 1990.
30. Lietti, L., Ramis, G., Berti, F., Toledo, G., Robba, D., Busca, G., and Forzatti, P., *Catal. Today* **42**, 101 (1998).
31. Lide, D. R., and Kehiaian, H. V., "The CRC Handbook of Thermophysical and Thermochemical Data" CRC Press, London, 1994.
32. Krogh Andersen, I. G., Krogh Andersen, E., Norby, P., and Skou, E., *J. Solid State Chem.* **113**, 320 (1994).
33. Decorse, P., Caboche, G., and Dufour, L.-C., *Solid State Ionics* **117**, 161 (1999).
34. Krogh Andersen, I. G., private communication.
35. Nowotny, D., and Rekas, M., *J. Am. Ceram. Soc.* **81**(1), 67 (1998).
36. Carter, S., Selcuk, A., Chater, R. J., Kajda, J., Kilner, J. A., and Steele, B. C. H., *Solid State Ionics* **53–56**, 597 (1992).
37. Ozawa, M., Toda, H., and Suzuki, S., *Appl. Catal. B: Environ.* **8**, 141 (1996).
38. Torre-Abreu, C., Ribeiro, M. F., Henriques, C., and Ribeiro, F., *Catal. Lett.* **43**(1–2), 31 (1997).
39. Inui, T., Iwamoto, S., Kojo, S., Shimizu, S., and Hirabayashi, T., *Catal. Today* **22**, 41 (1994).
40. Iwamoto, H., *Stud. in Surf. Sci. Catal.* **84**, 1395 (1994).
41. Komatsy, K., Nunokawa, M., Moon, I. S., Takahara, T., Namba, S., and Yashima, T., *J. Catal.* **148**, 1994 (1991).